Elliptical Dielectric Resonator Antenna for Dual-Band Operation

A. TADJALLI, A. SEBAK and T. DENIDNI*
ECE Dept, Concordia University, Montreal, QC, H3G 1M8, CANADA

* INRS-EMT, 800 de la Gauchetiere, Montreal, QC, H5A 1K6, CANADA

Abstract- This paper presents a new dual-band elliptical dielectric resonator antenna (EDRA). The EDRA is mounted on a ground plane and fed with a rectangular slot exited by a microstrip line. By optimizing the structure parameters, it is possible to obtain more than one excited mode in a limited frequency band. Numerical and measurement results for the radiation patterns of this slot fed EDRA are given and compared. A good agreement is obtained between numerical and measurement results.

Key-Words: - Elliptical dielectric resonator antenna, dual-band, Rayleigh-Ritz.

1 Introduction

Open dielectric resonators are potentially useful antenna elements. They offer several attractive features such as small size, high radiation efficiency, compatibility with MIC's, intrinsic mechanical simplicity, and the ability to control their radiation patterns using different modes [1]-[3]. Many of concepts used in the microstrip antenna design can also be applied in the dielectric resonator antenna design. Elliptically shaped structures have found increasing applications in several kinds of antennas, including microstrip antennas and a dielectric resonator antennas (DRAs) [4]-[6]. In particular, the elliptic geometry is becoming more popular since it allows a better control of the polarization characteristics and facilitates the design by changing both eccentricity and focal length to tune the parameters of interest. EDRAs are good candidates of small antennas for different wireless systems. The coupling between a rectangular waveguide feed and elliptical cavities ought to excite more propagating modes compared to coupling to rectangular cavities [7]. There is no mode splitting or rotation of the polarization plane for slight deformations of the cross section while simple matched connecting parts to rectangular and circular waveguides are possible [8]. For the analysis of such devices, the homogeneous Helmholtz equation in the elliptic coordinates is employed. Solving field problems of structures with elliptical geometries requires the computation of Mathieu and modified Mathieu functions [9]. These are the eigen solutions of the wave equation in elliptical coordinates. The analytical development of the solution for the excitation modes and far field patterns of EDRAs have been presented in reference [11]. Recently, more accurate results are also obtained by combining a perfect magnetic conductor (PMC) wall approximation with a special Green's function to analyze the proposed EDRA. The studies presented in this paper are focused on the analysis and design of a new dual-band operation EDRA. Both simulated and measured far-field patterns are presented and discussed in the following sections.

2 Antenna Geometry

The geometry of the slot coupled EDRA is shown in Fig. 1. The EDRA is fabricated from a powder of ceramic material of dielectric constant ε_r=12. In reference to Fig. 1, a and b are the semi-minor and semi–major radii of the ellipse, respectively, g_x (80mm) and g_y (80mm) are x and y dimensions of the ground plane. The height of the EDR is denoted by h. The EDRA is excited by a microstrip line through a narrow rectangular slot. The slot is etched on a microwave substrate with dielectric constant = 2.2 and thickness (t) = 1.5 mm. The microstrip line is terminated with an open-circuited stub of length l_m long beyond the x-axis, width w_m, and d_m is its offset from the ellipse center.

The coupling rectangular slot has a length l_s and width w_s. Slot has ($-d_m$, d_s) offset from the ellipse center. The EDRA fabricated with a copper-clad 1.5-mm dielectric sheet from Rogers Corporation, and the powder of dielectric. To shape the powder, foam with $\varepsilon_r \approx 1$ is used. Photographs of the antenna are shown in Fig. 2.

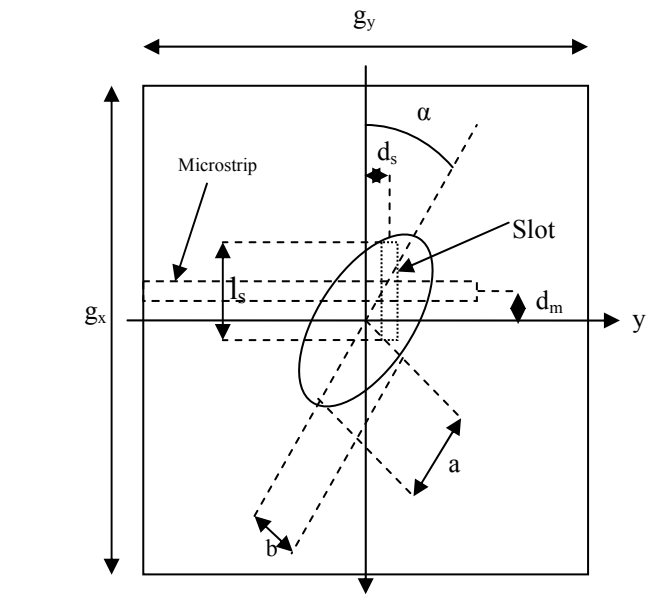

Fig. 1. Schematic diagrams of the proposed EDRA. (a) Top view. (b) Side view.

3 Analysis and Design of EDR

The solution of the wave equation for elliptical dielectric resonator (EDR) is investigated in this section. The EDR is mounted on a ground plane. a and b are the semi-major and semi-minor axes, respectively and h is the height. Image theory can be immediately applied where the ground plane is replaced by an image portion of the cylinder extending to $z = -h$. For a DR with very large dielectric permittivity, the dielectric-air interface can be approximated by a hypothetical perfect magnetic conductor (PMC), which requires that the tangential components of the magnetic field vanish on that surface.

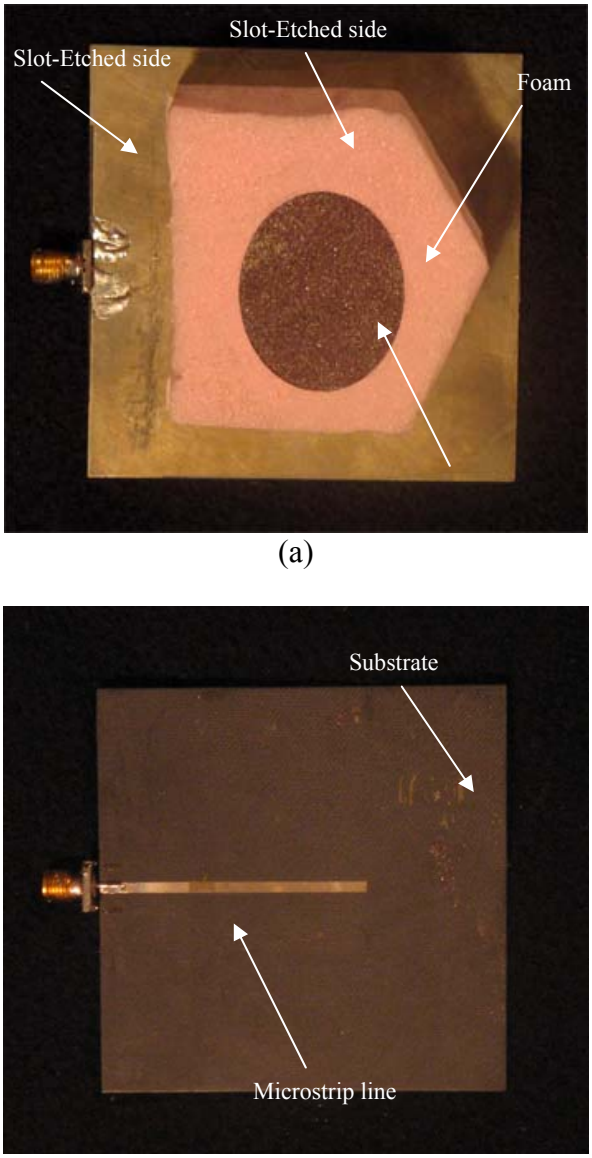

Fig. 2. Photograph of the fabricated slot-coupled EDRA (a) Top view (b) Bottom view

In elliptical coordinate the scalar Helmholtz equation is [10]:

$$\frac{2}{f_o^{\,2}(\cosh 2\xi - \cos 2\eta)}\left(\frac{\partial^2}{\partial \xi^2}+\frac{\partial^2}{\partial \eta^2}\right)\begin{Bmatrix}E_z\\H_z\end{Bmatrix}+(k^2-k_z^2)\begin{Bmatrix}E_z\\H_z\end{Bmatrix}=0 \quad (1)$$

Assuming that $E_z(H_z)$ can be written in the form of $R(\xi,g).S(\eta,g).\begin{bmatrix} Sin(k_z z) \\ Cos(k_z z) \end{bmatrix}$, we can rewrite (1) as

$$\frac{1}{R}\frac{\partial^2 R}{\partial \xi^2}+\frac{k^2-k_z^2}{2}f_o^{\,2}\cosh 2\xi=\frac{1}{S}\frac{\partial^2 S}{\partial \eta^2}-\frac{k^2-k_z^2}{2}f_o^{\,2}\cos 2\eta \quad (2)$$

where R and S are, respectively, the radial and angular Mathieu function, ξ is the radial coordinate and takes the values $\xi \in [0, \infty)$, and the coordinate η is an angular coordinate taking the range $\eta \in [0,2\pi)$. k is the wavenumber of EDR and k_z is the wave number of the EDR in z direction. The left- and right-hand sides of (2) must be equal to a separation constant, g. We can rewrite (2) as

$$\frac{\partial^2 S}{\partial \eta^2}+(g-2q\cos 2\eta)S=0 \quad (3)$$

$$\frac{\partial^2 R}{\partial \xi^2}-(g-2q\cosh 2\xi)R=0 \quad (4)$$

$$q\equiv\frac{k_c^2}{4}f_o^{\,2} \quad (5)$$

where $k_c=\sqrt{k^2-k_z^2}$ is the elliptical cross-section wavenumber and f_o is semi-focal distance of ellipse.

The expressions for the TE^z and TM^z modes may be written as follows:

TE^z Modes:

$$H_z(\xi,\eta,z)=\sum_{n=0}^{\infty}\sum_{m=0}^{\infty}\sum_{p=0}^{\infty}\{A_{e_{nmp}}^{TE}R_{e_{nm}}^{TE}(q_{e_{nm}}^{TE},\xi)S_{e_{nm}}^{TE}(q_{e_{nm}}^{TE},\eta)+A_{o_{nmp}}^{TE}R_{o_{nm}}^{TE}(q_{o_{nm}}^{TE},\xi)S_{o_{nm}}^{TE}(q_{o_{nm}}^{TE},\eta)\}\sin(k_{z_p}z) \quad (6)$$

TM^z Modes:

$$E_z(\xi,\eta,z)=\sum_{n=0}^{\infty}\sum_{m=0}^{\infty}\sum_{p=0}^{\infty}\{A_{e_{nmp}}^{TM}R_{e_{nm}}^{TM}(q_{e_{nm}}^{TM},\xi)S_{e_{nm}}^{TM}(q_{e_{nm}}^{TM},\eta)+A_{o_{nmp}}^{TM}R_{o_{nm}}^{TM}(q_{o_{nm}}^{TM},\xi)S_{o_{nm}}^{TM}(q_{o_{nm}}^{TM},\eta)\}\sin(k_{z_p}z) \quad (7)$$

where $A_{o_{nmp}}^{TE}$, $A_{e_{nmp}}^{TE}$, $A_{e_{nmp}}^{TM}$ and $A_{o_{nmp}}^{TM}$ are unknown expansion coefficients. We will use the subscript e and o to refer to even and odd modes respectively.

For both TE and TM waves, the boundary conditions are given by:

$$H_\eta(\xi=\xi_0,-1\le\eta\le 1,0\le z\le h)=0 \quad (8a)$$

$$H_\eta(1\le\xi\le\xi_0,-1\le\eta\le 1,z=h)=0 \quad (8b)$$

$$H_\xi(1\le\xi\le\xi_0,-1\le\eta\le 1,z=h)=0 \quad (8c)$$

$$H_z(\xi=\xi_0,-1\le\eta\le 1,0\le z\le h)=0 \quad (8d)$$

$$E_\eta(1\le\xi\le\xi_0,-1\le\eta\le 1,z=0)=0 \quad (8e)$$

$$E_\xi(1\le\xi\le\xi_0,-1\le\eta\le 1,z=0)=0 \quad (8f)$$

where ξ_0 defines the lateral surface of EDR. Using the boundary condition (8c) gives the resonant frequencies and can be written in the form

$$\cos(k_z h)=0\rightarrow k_{z_p}=\frac{(2p+1)\pi}{2h};\ p=0,1,2,... \quad (9)$$

$$f_{e_{o_{nmp}}^{(TM)}}^{(TE)}=\frac{c}{2\pi\varepsilon_r}\sqrt{k_{c_{e_{o_{nm}}^{(TM)}}}^{(TE)2}+k_{zp}^2} \quad (10)$$

where c is velocity of light, ε_r is the permittivity of dielectric and is $k_{c_{e_{o_{nm}}^{(TM)}}}^{(TE)}$ the elliptical cross-section wavenumber. The cutoff wavenumbers are obtained by setting the functions or their derivatives, depending on the boundary conditions in (8). Since fields should be single valued then the first boundary condition is given by

$$\begin{bmatrix} E \\ H \end{bmatrix}(\xi,\eta,z)=\begin{bmatrix} E \\ H \end{bmatrix}(\xi,\eta+2\pi,z) \quad (11)$$

and the use of Mathieu function $S_{e_{o_{nm}}^{(TM)}}^{(TE)}(q_{mn}^{(TM)},\eta)$ is appropriate in this case. The elliptic boundary of the membrane is given by $\xi=\xi_0$=constant, and the eccentricity e of the ellipse is defined as

$$e=\frac{f_o}{a}=\frac{1}{\cosh\xi_0} \quad (12)$$

On the elliptic boundary ($\xi=\xi_0$) the membrane is fixed, therefore:

$$TE:\quad R_{e_{o_n}}(\xi_0)=0 \quad (13)$$

$$TM:\quad \left.\frac{\partial R_{e_{o_n}}(\xi)}{\partial\xi}\right|_{\xi=\xi_0}=0 \quad (14)$$

If we choose a certain harmonic n we have an infinite set of possible values of q that satisfy (13) and (14). Let q^{TE}_{nm} the m-th zero of R of n-order and q^{TM}_{nm} the m-th zero of derivative of R of the n-th-order. According to (8), for each q^{TE}_{nm} or each q^{TM}_{nm} there

exists a corresponding frequency f^{TE}_{nm} or f^{TM}_{nm}. Solving (5) for resonant frequencies leads to

$$f^{(TE\atop TM)}_{e\atop o\,nmp} = \frac{c}{2\pi\varepsilon_r}\sqrt{\frac{4q^{(TE\atop TM)}_{mn}}{f_o^2}+k_{zp}^2} \tag{15}$$

Except for the first harmonic n = 0, all modes can be even or odd. Some numerical results were shown in [10]. The confocal annular elliptic structure is a very versatile configuration and offers a reasonable controllability over the positions of its resonant modes. The eigen-function of elliptical cylinder dielectric resonator can be expressed in the form:

$$\psi_{e\atop o\,mnp}(x,y,z) = \begin{bmatrix} Ce_m(\xi,q_n)ce_m(\eta,q_n) \\ Se_m(\xi,q_n)se_m(\eta,q_n) \end{bmatrix}\cos(k_{zp}z) \tag{16}$$

Where $k_{zp} = \dfrac{(2p+1)\pi}{2h}$; $p = 0,1,2,...$ Subsequently, the Green's function of EDRA can be written

$$G(x,y,z;x',y',z') = \sum_{m=1}^{\infty}\sum_{n=0}^{\infty}\sum_{p=0}^{\infty}\frac{\psi_{mnp}(x,y,z)\psi_{mnp}(x',y',z')}{T_{mnp}} \tag{17}$$

and T_{mn} is the normalization factor.

$$T_{mnp} = \int_1^{\xi_0}\int_0^{2\pi}\int_{-h}^{h}\psi_{mnp}^2[\cosh 2\xi - \cos 2\eta]dzd\eta d\xi \tag{18}$$

The radiation patterns of the EDRA are calculated using a two-step process. In the first step the electric field integral equation for the current distribution on the slot is formulated in terms of the specialized Green's functions (17). The integral equation is then solved using the method of moments with piecewise sinusoidal bases and testing functions. In the second step, once the current distribution on the slot is computed, both the electric and magnetic fields inside the cavity are calculated in terms of the magnetic vector potential A.

$$A_z(\xi,\eta,z) = \sum_{m=0}^{\infty}\sum_{n=1}^{\infty}\int_{-l}^{l} I(\xi',\eta',z')G(\xi',\eta',z';\xi,\eta,z)dz' \tag{19}$$

The surface magnetic current on the cavity walls is defined as

$$\vec{M} = \vec{E}\times\hat{n} \tag{20}$$

where $\hat{n}$ is a unit normal pointing out of the dielectric. The electric vector potential is then expressed as

$$\vec{F} = \frac{\varepsilon}{4\pi}\iint_S \vec{M}_s(r')\frac{e^{-jk_0R}}{R}ds' \tag{21}$$

where R represents the distance from any point on the EDR to the observation point. The far electric field components are then obtained using

$$E_\varphi = +j\omega F_\theta \tag{22.a}$$

$$E_\theta = -j\omega F_\varphi \tag{22.b}$$

4 Results

By carefully adjusting the slot position and dimensions, the EDRA can operate at different bands. Measured Return loss of an EDRA with a=18mm, b=23.4, l_m=12mm, w_m=2mm, d_m=-3mm, l_s=25mm, w_s=2.4mm, d_s=0 and h=30mm is shown in Fig. 3. It can be observed that the measured center frequencies are 4.635GHz and 4.840GHz. Additionally, the simulated bandwidths for a return loss below -10dB are 25MHz in the lower band and 55MHz in the upper band. Next, the far-field radiation patterns of the EDRA were simulated using the theory presented in [10]. The radiation patterns are also measured at the resonant frequencies. The results are shown in Figs. 4 and 5. In the simulation, the ground plane is considered infinite. In general, a good agreement is noticed between the numerical and measurement results. The asymmetrical nature of the radiation pattern is due to the influence of higher order modes. At 4.635 GHz, it can be observed from Fig. 4 that the radiation pattern for the upper side of the ground plane is almost omni – directional except two nulls at $(\theta,\varphi)=(30^0,90^0)$ and $(30^0,270^0)$. At the higher frequency, 4.840GHz, the far-field patterns, shown in Fig. 5, are similar to the patterns at 4.635GHz but with a higher gain at θ-values close to 0^0.

As shown in Fig. 3 for the elliptical case, we can easily obtain two resonant frequencies close to each other by controlling a/b. This property is very valuable to generate circular polarization (CP) and

wide band operation. For example, the EDRA with h=29mm, l_m=25mm, l_s=18mm, w_s=1.5mm, α (angular offset of EDR around z-axis) =15^0, a=14.97mm, b=20.96mm, g_x=g_y=80mm, and t=1.5mm is designed to generate CP. Fig. 6 plots the return loss of the EDRA and clearly shows the two resonances of the modes even TE_{020} **[11]** and odd TE_{110}. Fig. 7 shows the corresponding AR. It is observed that the -3dB CP axial ratio (AR) bandwidth is 2.7%, which is reasonable for a single-fed CP EDRA. The xz and yz planes radiation patterns at 3.03GHz are displayed in Fig. 8, where broadside field patterns are observed, as expected.

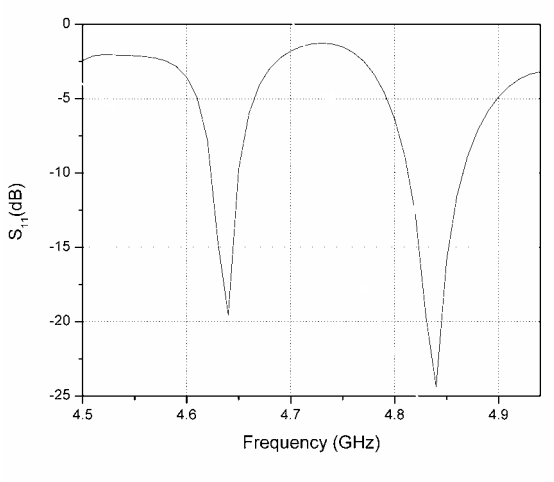

Fig. 3. Return Loss Response

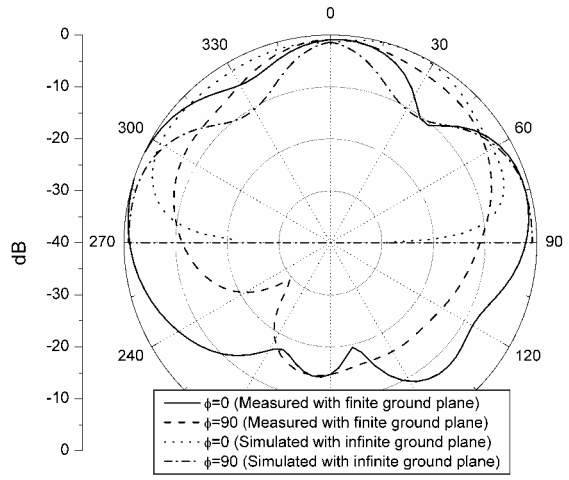

Fig. 4. Simulated and measured radiation patterns of the proposed antenna operating at 4.635GHz.

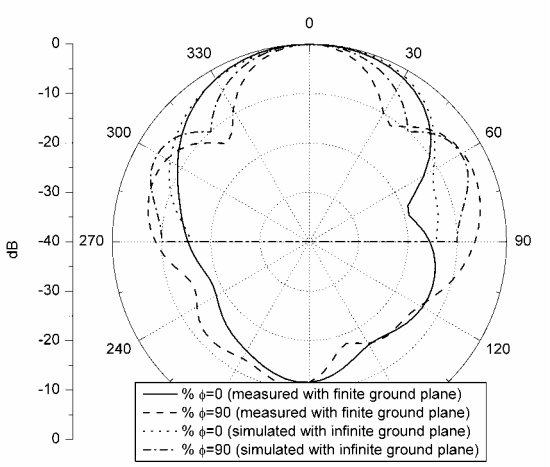

Fig. 5. Simulated and measured radiation patterns of the proposed antenna operating at 4.840GHz.

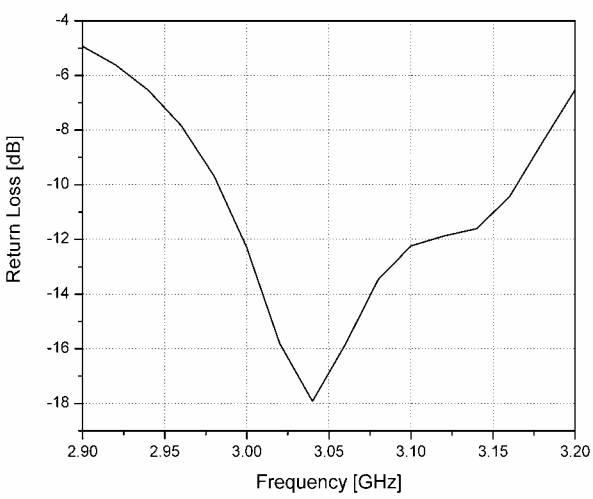

Fig. 6. Return Loss of the Designed Circular Polarized EDRA

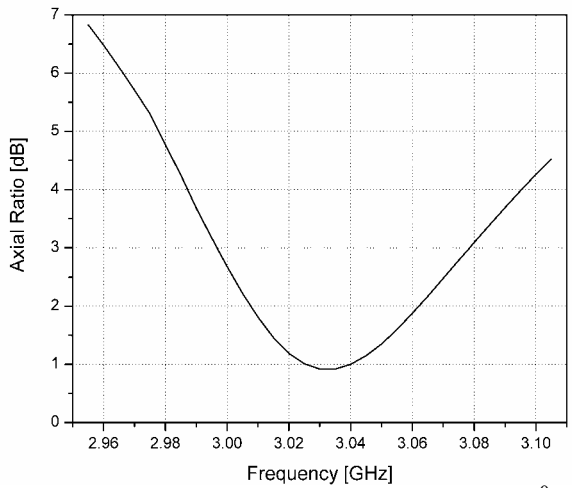

Fig. 7. Axial Ratio of the EDRA at θ=0^0

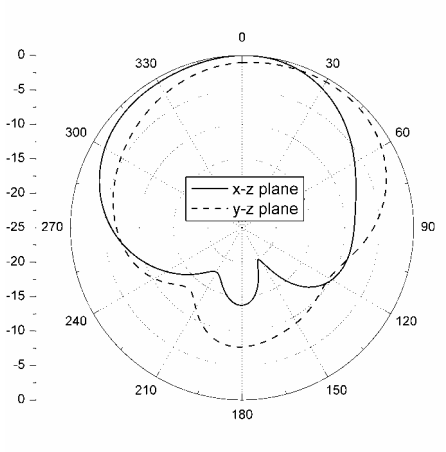

Fig. 8. Far Field Pattern of the EDRA at 3.03 GHz

5 Conclusion

A new EDRA for a close dual-band operation has been presented in this letter. Calculated and measured far-field patterns are compared well with a good agreement at both frequencies. The results show the flexibility of EDRAs to generate dual-band operation. Finally, an example has been presented to show an EDRA, which has two resonant modes close to each other to generate CP.

References:

[1] R.K. Mongia, and P. Bhartia, Dielectric resonator antennas—A review and general design relations for resonant frequency and bandwidth, *Int. J. Microwave Millimeter-Wave Eng.*, vol. 4, July 1994, pp. 230–247.

[2] R.K. Mongia, A. Ittipiboon, and M. Cuhaci, Measurement of radiation efficiency of dielectric resonator antennas, *IEEE Microwave Guided Wave Lett.*, vol. 4 Mar. 1994, pp. 80–82,.

[3] A. Petosa, A. Ittipiboon, Y. M. M. Antar, D. Roscoe, and M. Cuhaci, Recent advances in dielectric resonator antenna technology, *IEEE Antennas Propagat. Mag.*, vol. 40, June 1998, pp. 35–48.

[4] A. K. Bhattacharyya and L. Shafai, Theoretical and experimental investigation of the elliptical annual ring antenna, *IEEE Trans. Antennas Propagat.*, vol. AP-36, no. 11, Nov. 1988, pp. 1526-1530.

[5] Y. Hu, F. M. Ghonnouchi and R. G. Bosisio, Theoretical and experimental measurement of microwave permittivity using open ended elliptical coaxial probes, *IEEE Trans. Microwave Theory Tech.,* vol. MTT-40, Jan. 1992, pp. 143-150.

[6] K. Sun and J. M. Tranquilla, Study of elliptical annular microstrip antenna using full Mathieu formulation, IEEE Intern. Symp. On Antennas and Propagat., vol-AP-S-2, 1994, pp. 944-947.

[7] A. Morini,T. Rozzi,M. Pistolesi,F. Spinsanti, Variational analysis of arbitrarily oriented thick iris coupling a rectangular and an elliptical waveguide, *IEEE MTT-S International symposium* ,Vol. 3, 8-13 June 1997, pp.1243 - 1246.

[8] J. G. Kretzschmar, Wave Propagation in Hollow Conducting Elliptical Waveguides, *IEEE Transactions on Microwave Theory and Techniques*, Vol. 18, Issue 9, 1970, pp. 547 – 554.

[9] F. A. Alhargan, A complete method for the computations of Mathieu characteristic numbers of integer orders, *SIAM Rev.* 38, 2, 1996, pp. 239–255.

[10] A. Tadjalli, A. R. Sebak, and T. A. Denidni, Resonance Frequencies and Far Field Patterns of Elliptical Dielectric Resonator Antenna: Analytical Approach, *Progress In Electromagnetics Research*, PIER 64, 2006, pp. 81-98,.

[11] A. Tadjalli, A. R. Sebak, T. Denidni, Modes of Elliptical Cylinder Dielectric Resonator and its Resonant Frequencies, *IEEE AP-S International Symposium,* Vol. 2, Monterey, June 2004, pp. 2039-2042.